CHAPTER 4

Tau-p PROCESSING IN REAL SEISMIC DATA

4.1 Linear *tau-p* processing in real seismic data

Full linear *tau-p* processing steps (Figure 3.1) and residual static (Appendix B) are applied to the real data. Each processing steps and its parameters are presented in Table 4.1.

Table 4.1 Processing steps and parameters of real data in the linear *tau-p* processing.

Processing	Parameters
1.Geometry setting and static correction	
2.Trace editting and amplitude recovery	mute refracted wave and killed bad traces
3. *f-k* filtering	attenuated ground roll
4.CMP sorting	rearrange data (shot ⟶ CMP)
5.Supergather	3 CMPs to 1 Supergather
6.Forward linear *tau-p* processing	sample interval = 12.5 m, max, min *tau-p* slope = $\pm 750\times10^{-6}$ s/m, No. of slope = No. of trace input
7.HVF	k = 15%, velocity function *B.RealVel1*
8.Predictive deconvolution	n = 200 ms, α = 20 ms, ε = 0.1%
9.Filtering	5/10-55/60 Hz
10.Inverse linear *tau-p* processing	restore the input record
11.Velocity analysis1	output : velocity function *B.RealVel3*
12.Stacking1	output : brute stack section
13.Residual static correction	
14.Velocity analysis2	output : velocity function *B.RealVel4*
15.Stacking2	output : final stack section

The sequence for linear *tau-p* processing in Table 4.1 is described as follows:

Step 1, *Step 2* and *Step 3* are similar to the conventional processing in real data.

Step 4: Rearrange data from the common shot domain to the common mid point (CMP) domain (Figure 4.1).

Step 5: To improve the quality of seismic data. The number of seismic traces in CMP domain is increased from 30 trace to 120 trace (Figure 4.1 and 4.2).

Step 6: Transform seismic data *t-x* domain to linear *tau-p* domain where the parameters of the maximum *tau-p* slope are obtained from the minimum velocity of the velocity function from brute stack processing in Chapter 1 which is 1400 m/s, thus will obtain the maximum slowness (*1/v*) is $1/1400 \approx 750$ μs/m (Figure 4.3 (a)).

Step 7: Reduce aliasing problem between the transformations. The HVF is designed from equation (2.35) by applied velocity function *B.RealVel1* from the conventional processing, result is shown in Figure 4.3 (b).

Step 8: To eliminate multiples in the linear *tau-p* domain where all parameters are designed from auto-correlation and tested by a trial-error method.

Step 9: After applying predictive deconvolution, the bandpass filter is applied (Figure 4.4 (a)).

Step 10: Transform data in linear *tau-p* domain back to *t-x* domain by using the same input parameter, output is shown in Figure 4.4 (b).

Step 11: After linear *tau-p* processing, it is often necessary to examine the new velocity analysis to obtain the improved velocity function (*B.RealVel3* ; Figure 4.5).

Step 12: The new velocity function *B.RealVel3* is applied for NMO correction and follow by stacking. The result is shown stack section in Figure 4.6.

Step 13: After topographic correction is applied, most of small time shifts between traces remained. To correct for these small shifts the residual static correction is applied.

Step 14: After residual static correction is applied, there are relative static shifts from CMP gather. It is often necessary to pick the new velocity function (*B.RealVel4*) again.

Step 15: Applied NMO correction in the CMP records after applying residual static correction by using velocity function *B.RealVel4* and then stack to obtain the final stack section (Figure 4.7).

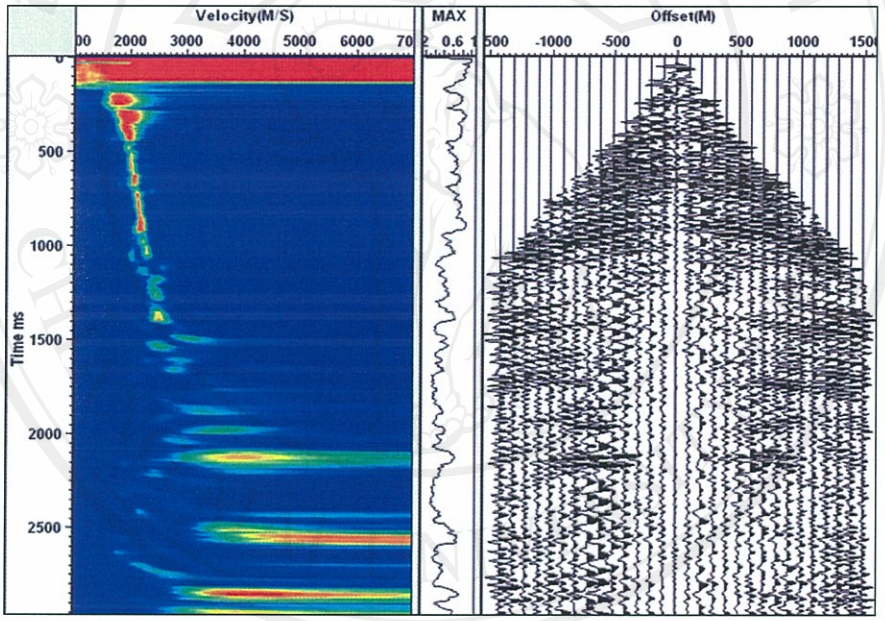

(a) (b)

Figure 4.1 (a) Velocity energy spectrum of CMP 339 before supergather. (b) CMP 339 before supergather (30 traces).

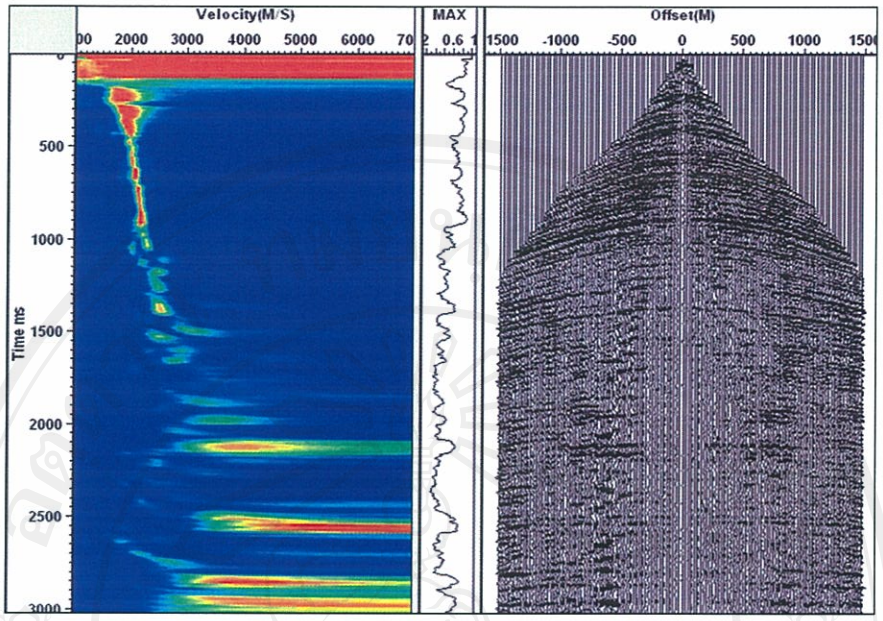

(a) (b)

Figure 4.2 (a) Velocity energy spectrum of CMP 339 after supergather. (b) CMP 339 after supergather that 3 CMPs to 1 Supergather (120 traces).

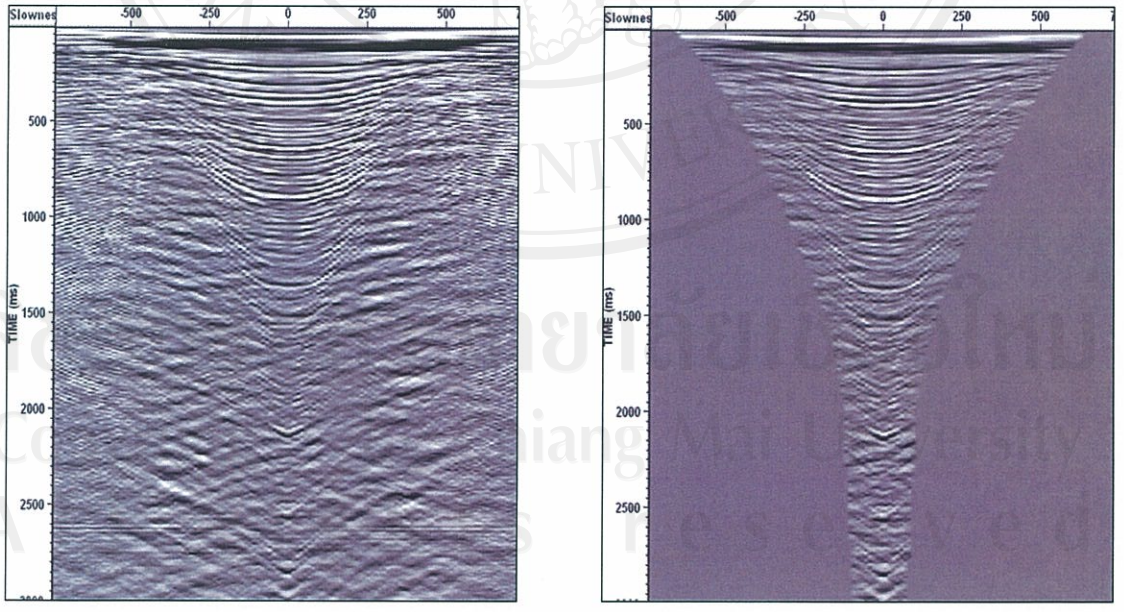

(a) (b)

Figure 4.3 (a) Forward linear *tau-p* transformation. (b) HVF is applied to mute aliasing in linear *tau-p* domain. The horizontal axis is slowness (p) in $\times 10^{-6}$ s/m and the vertical axis is interceptime (τ) in ms.

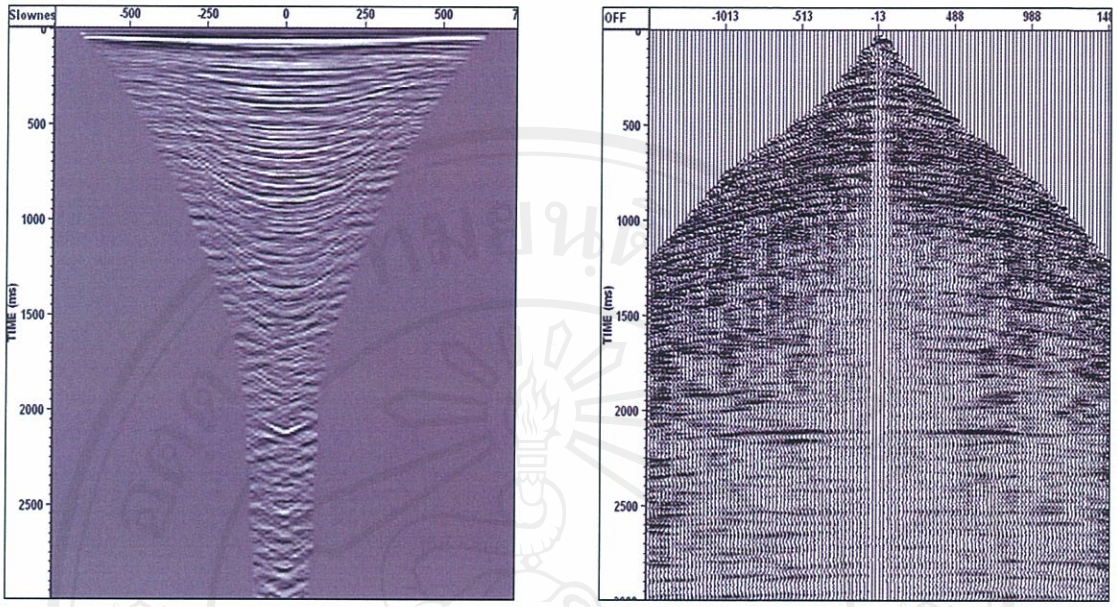

(a) (b)

Figure 4.4 (a) The deconvolution in linear *tau-p* domain where the horizontal axis is slowness (p) in $\times 10^{-6}$ s/m and the vertical axis is interceptime (τ) in ms. (b) Inverse linear *tau-p* transformation.

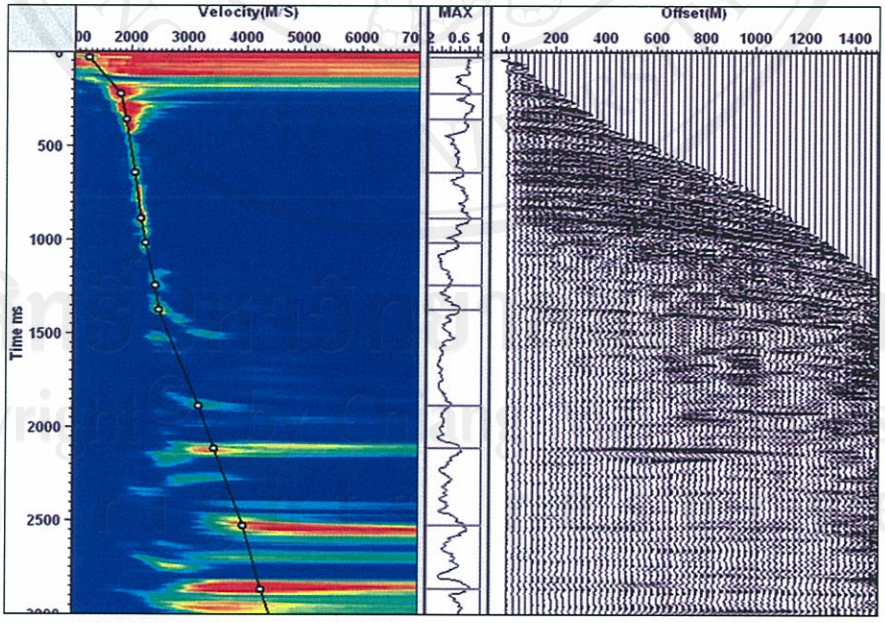

Figure 4.5 Velocity analysis of linear *tau-p* processing in real data, (left) the semblance analysis where the black line is velocity picking and the common offset stacking (right).

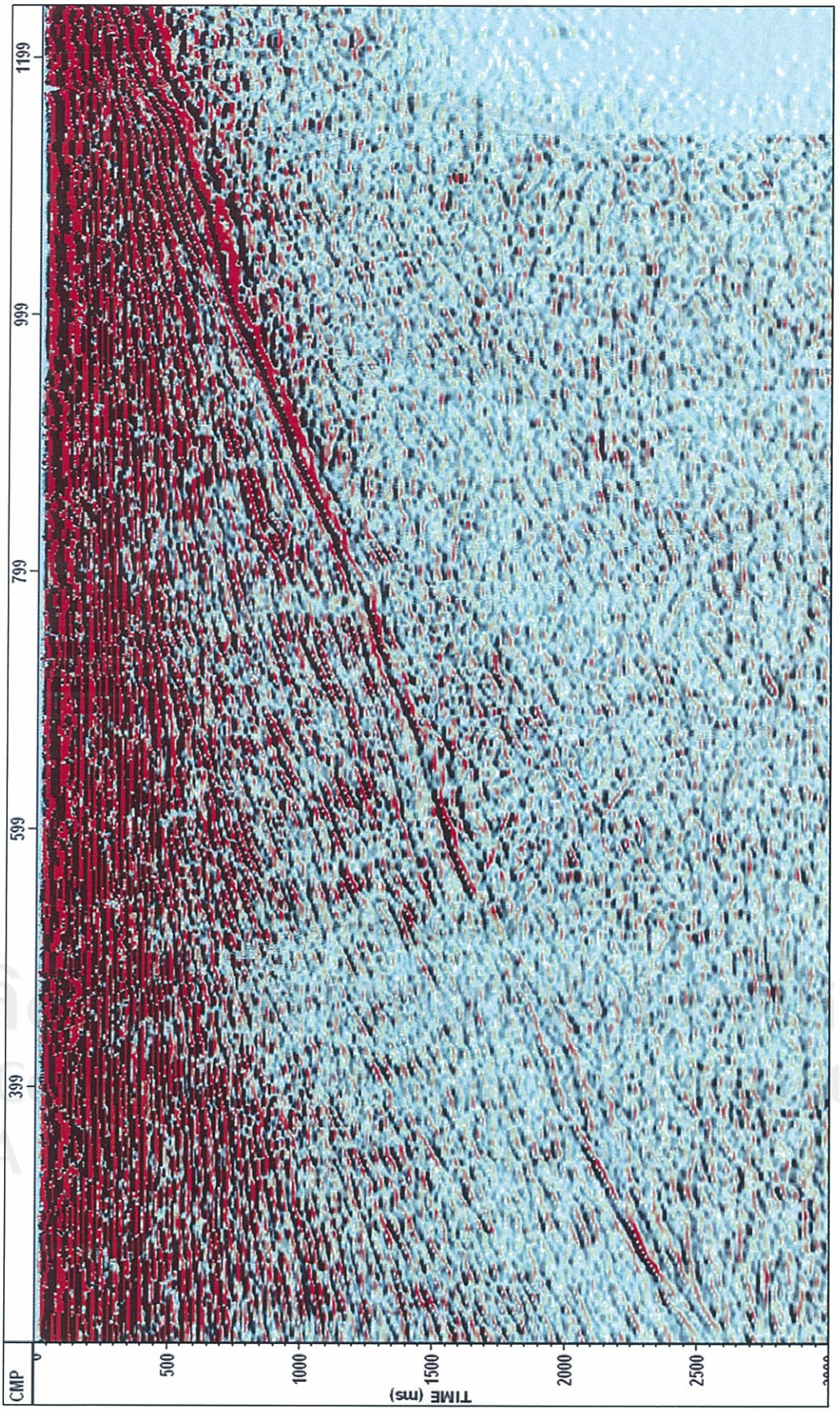

Figure 4.6 Stack section of real data after linear *tau-p* processing.

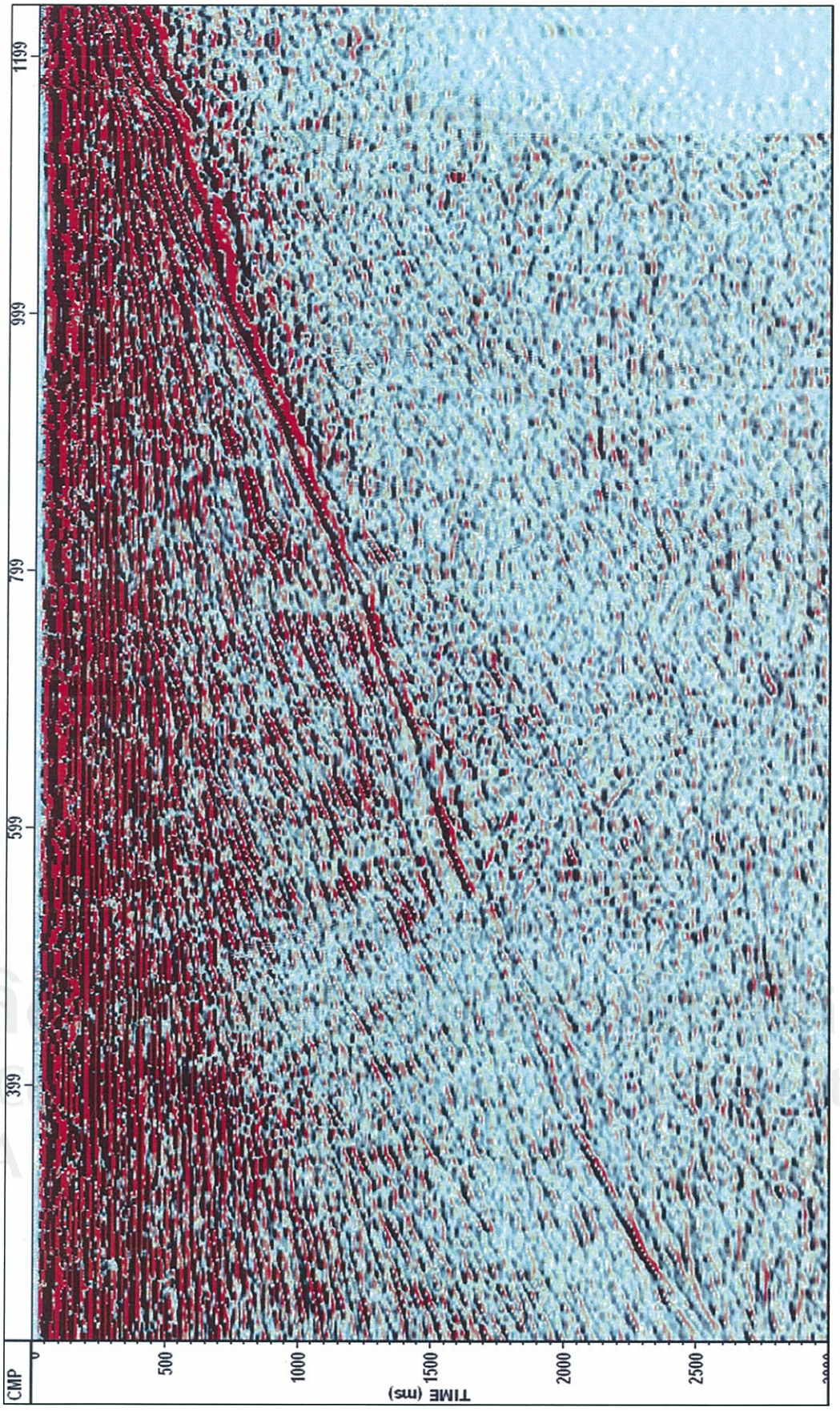

Figure 4.7 Residual static applied final stack section of real data after linear *tau-p* processing.

4.2 Parabolic *tau-p* processing in real seismic data

Full parabolic *tau-p* processing steps (Figure 3.1) and residual static (Appendix B) are applied to the real data. Each processing steps and its parameters are presented in Table 4.2.

Table 4.2 Processing steps and parameters of real data in the parabolic *tau-p* processing.

Processing	Parameters
1.Geometry setting and static correction	
2.Trace editting and amplitude recovery	mute refracted wave and killed bad traces
3. f-k filtering	attenuated ground roll
4.CMP sorting	rearrange data (shot ⟶ CMP)
5.NMO correction	by using velocity function *B.RealVel1*
6.Forward parabolic *tau-p* processing	- reference max offset : 1500 - max, min reference offset : ± 120 ms - moveout increment : 8 ms
7. Filtering	2/7-31/40 (antialiasing Equation 2.39)
8. Sign square	S/N enhanced
9.Multiple muting	
10.Inverse parabolic *tau-p* processing	- reference max offset : 1500 - max, min reference offset : ± 120 ms - moveout increment : 8 ms
11.Sign square root	energy preserved
12.Predictive deconvolution	n = 100 ms, α = 44 ms, ε = 0.1%
13.Filtering	2/7-31/36 Hz
14.Inverse NMO correction	by using velocity function *B.RealVel1*
15.Velocity analysis1	output : velocity function *B.RealVel5*
16.Stacking1	output : brute stack section
17.Residual static correction	
18.Velocity analysis2	output : velocity function *B.RealVel6*
18.Stacking2	output : final stack section

The sequence for parabolic *tau-p* processing in Table 4.2 is described as follows:

Step 1, *Step 2, Step3* and *Step4* are similar to linear *tau-p* processing.

Step 5: The NMO correction is applied by using velocity function *B.RealVel1* from the conventional processing in Chapter 1. The character of reflectors and

multiples are separated because the seismic from reflectors are flat and that from multiples are under-corrected (Figure 4.8 (a)).

Step 6: Transform data in *t-x* domain to parabolic *tau-p* domain (Figure 4.8 (b)). The maximum and the minimum parameters are designed and tested until clearly to analyze the signal and noise because it is not clearly to read maximum moveout time after NMO correction.

Step 7: The frequency aliasing are computed from Equation (2.39) where the maximum offset (x) is 1500 m, input trace spacing (Δx) is 100 m and the curvature (q) is 120 ms / 1500^2 m^2, thus we obtain the maximum frequency (f_{max}) is 31 Hz.

Step 8: Enhancing S/N by sign squaring all data in parabolic *tau-p* domain (Figure 4.9 (a)).

Step 9: The multiple muting is designed in parabolic *tau-p* domain and applied to all data (Figure 4.9 (b)).

Step 10: Transform data in parabolic *tau-p* domain back to *t-x* domain by using same input parameters, the result is presented in Figure 4.10 (a).

Step 11: Sign square root all data to preserve the relative amplitude variations after inverse parabolic *tau-p* transformation.

Step 12 After inverse parabolic *tau-p* transform, the predictive deconvolution is assigned to correct the energy of reflectors that is unsharpened and to attenuate remnant multiples.

Step 13: After applying deconvolution, the bandpass filter is applied.

Step 14: Inverse NMO correction is applied by using velocity function (*B.RealVel1* ; Figure 4.10 (b)).

Step 15: Semblance analysis, common offset stack and common velocity stack compose velocity analysis to obtain the velocity function (*B.RealVel5* ; Figure 4.11).

Step 16: The velocity function (*B.RealVel5*) is applied to the data in the NMO correction and followed stacking. The result is shown in brute stack section in Figure 4.12.

Step 17: After topographic correction is applied to the data, most of small time shifts between traces remained. The residual static correction is applied to correct for these small shifts

Step 18: After residual static correction is applied, relative static shifts from CMP gather. It is often necessary to examine the new velocity analysis (*B.RealVel6*).

Step 19: Applied NMO correction in the CMP records after applying residual static correction by using velocity function *B.RealVel6* and stacking to obtain the final stack section (Figure 4.13).

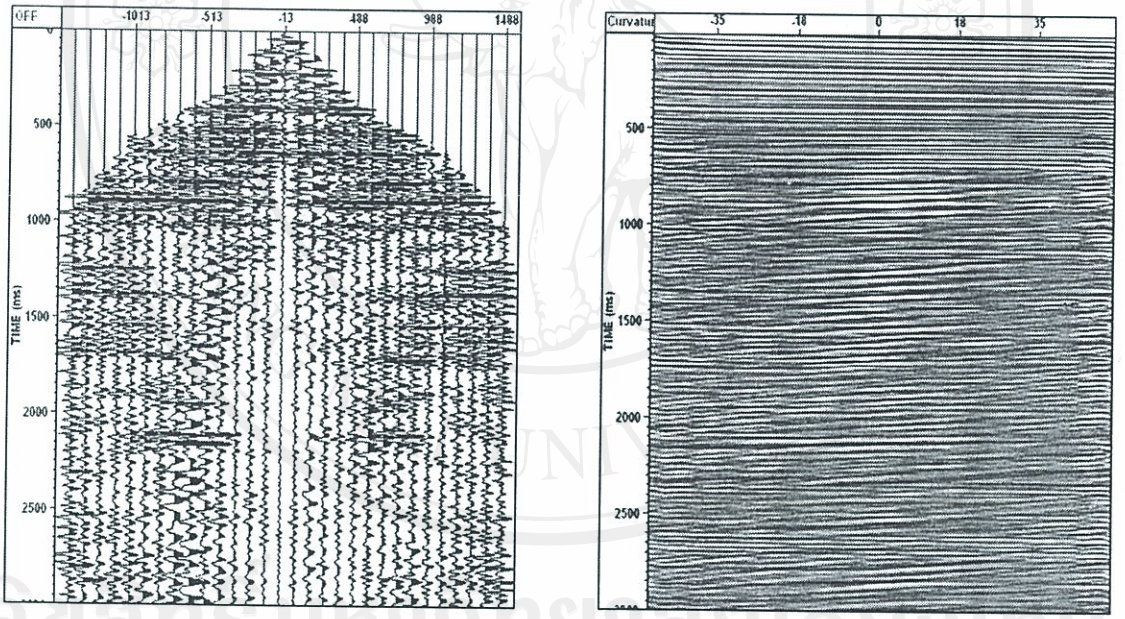

(a) (b)

Figure 4.8 (a) Applying NMO correction in CMP record by using velocity function *B.RealVel1*. (b) Forward parabolic *tau-p* transformation where the horizontal axis is curvature (q) in $\times 10^{-9}$ s/m^2 and vertical axis is intercept time (τ) in ms.

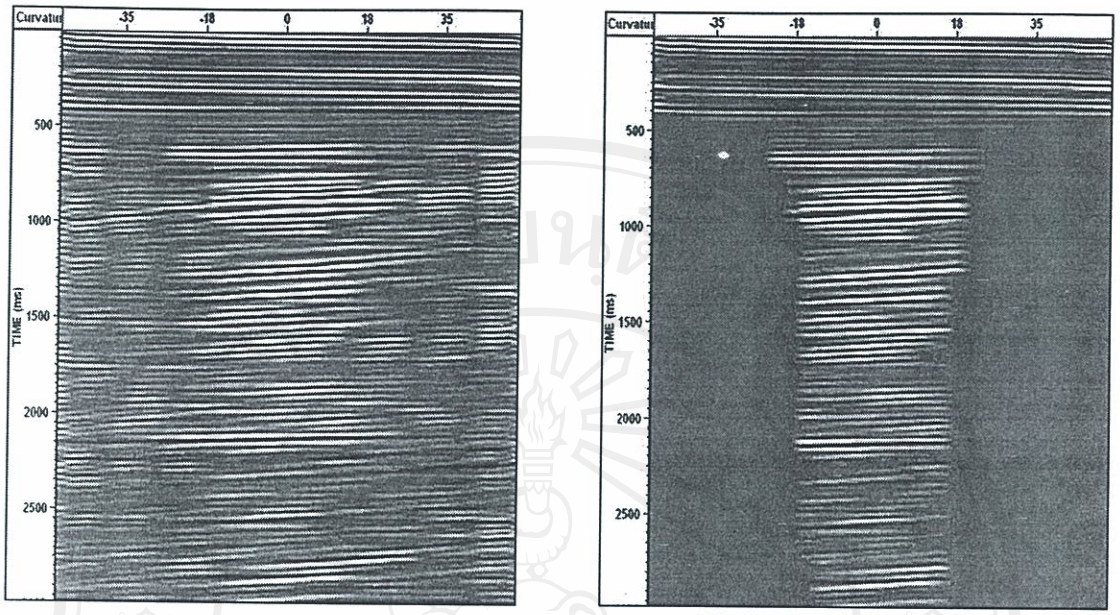

Figure 4.9 (a) Sign squaring all data in parabolic *tau-p* domain. (b) Multiple muting in parabolic *tau-p* domain.

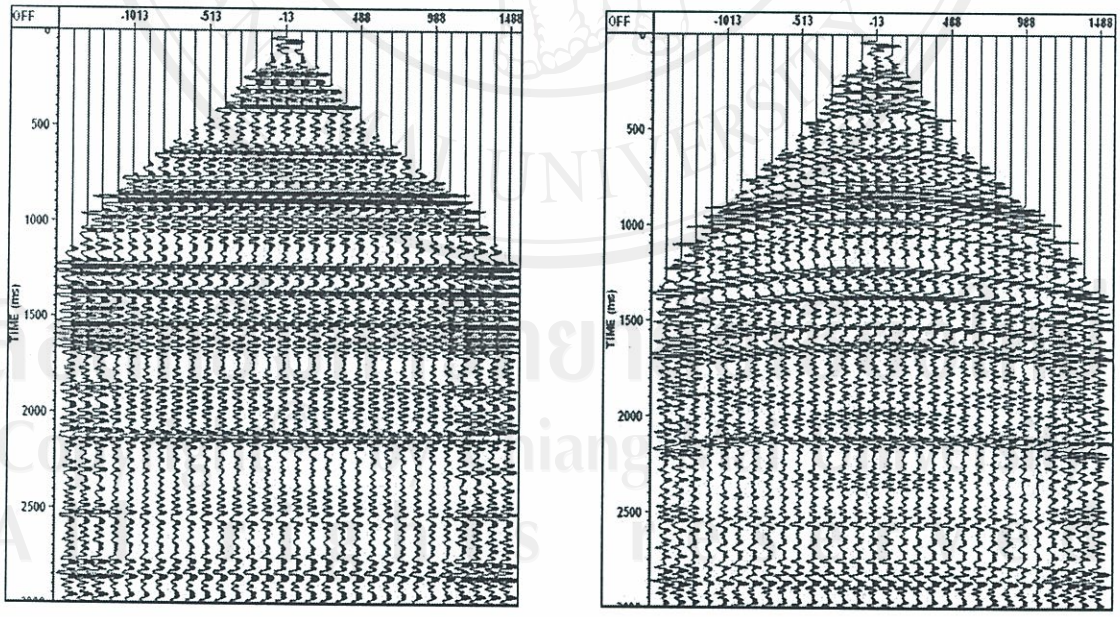

Figure 4.10 (a) Inverse parabolic *tau-p* transform and following sign square root. (b) Shot record after applied predictive deconvolution and inverse NMO.

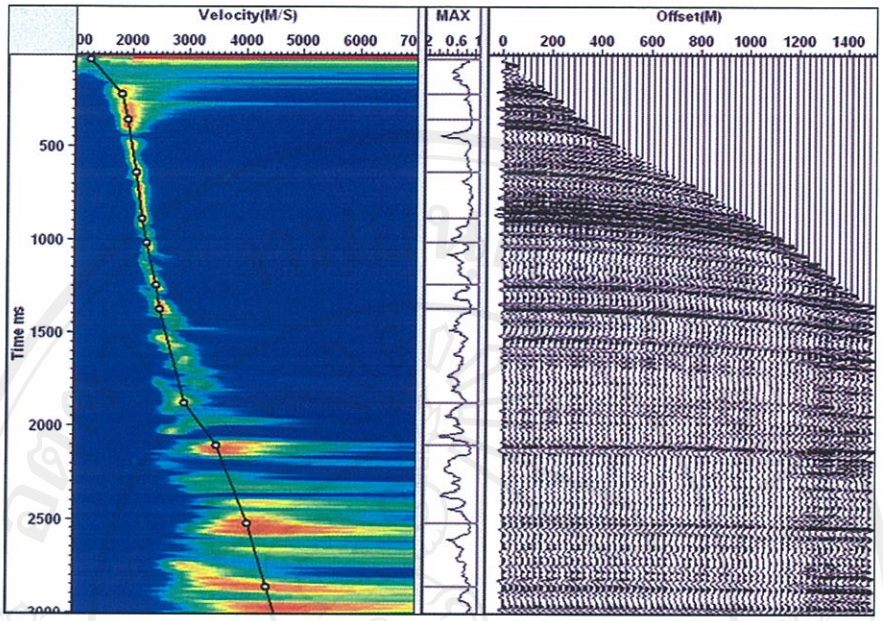

Figure 4.11 Velocity analysis of real data in parabolic *tau-p* processing, (left) the semblance analysis where the black line is velocity picking and the common offset stacking (right).

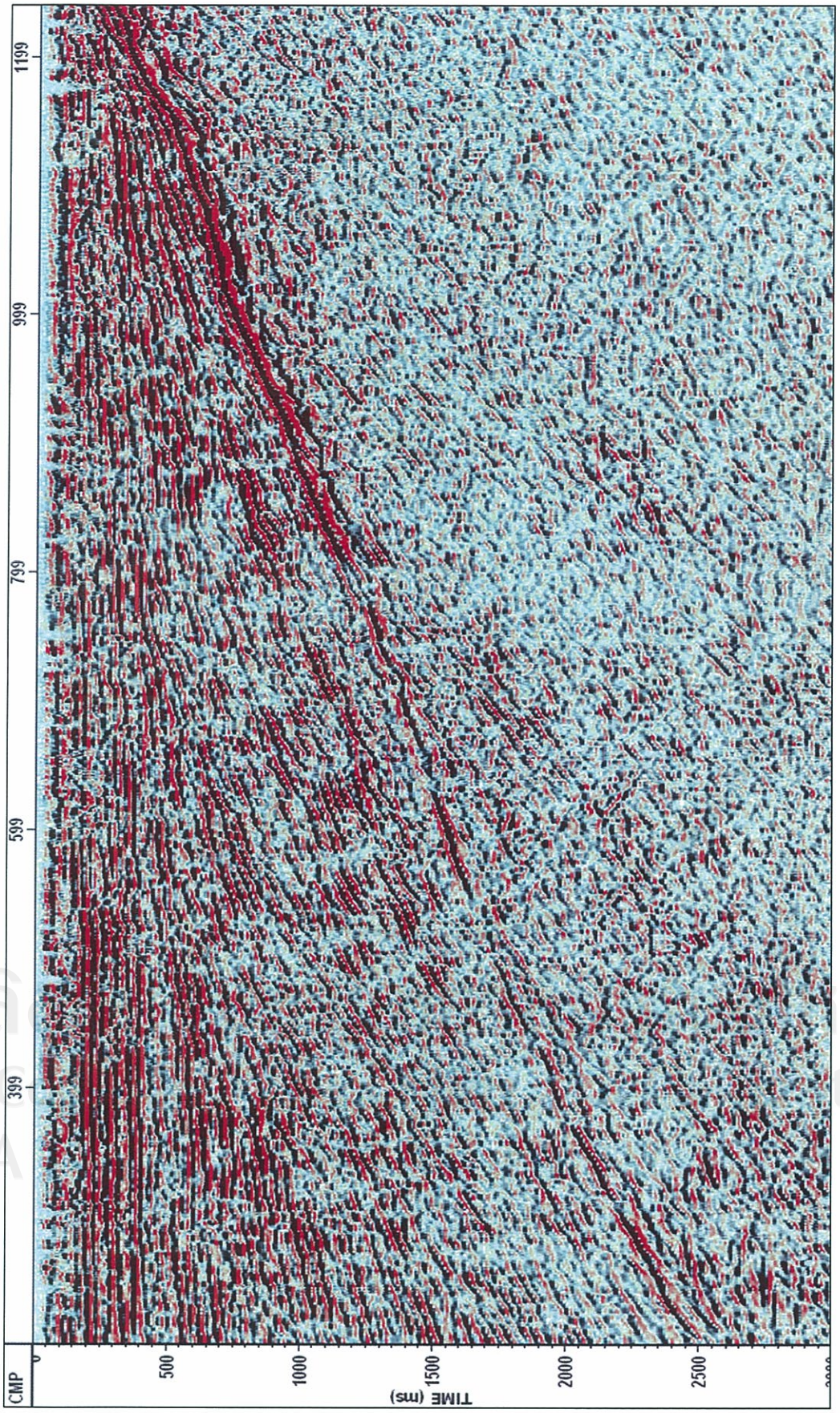

Figure 4.12 Stack section of real data after parabolic *tau-p* processing.

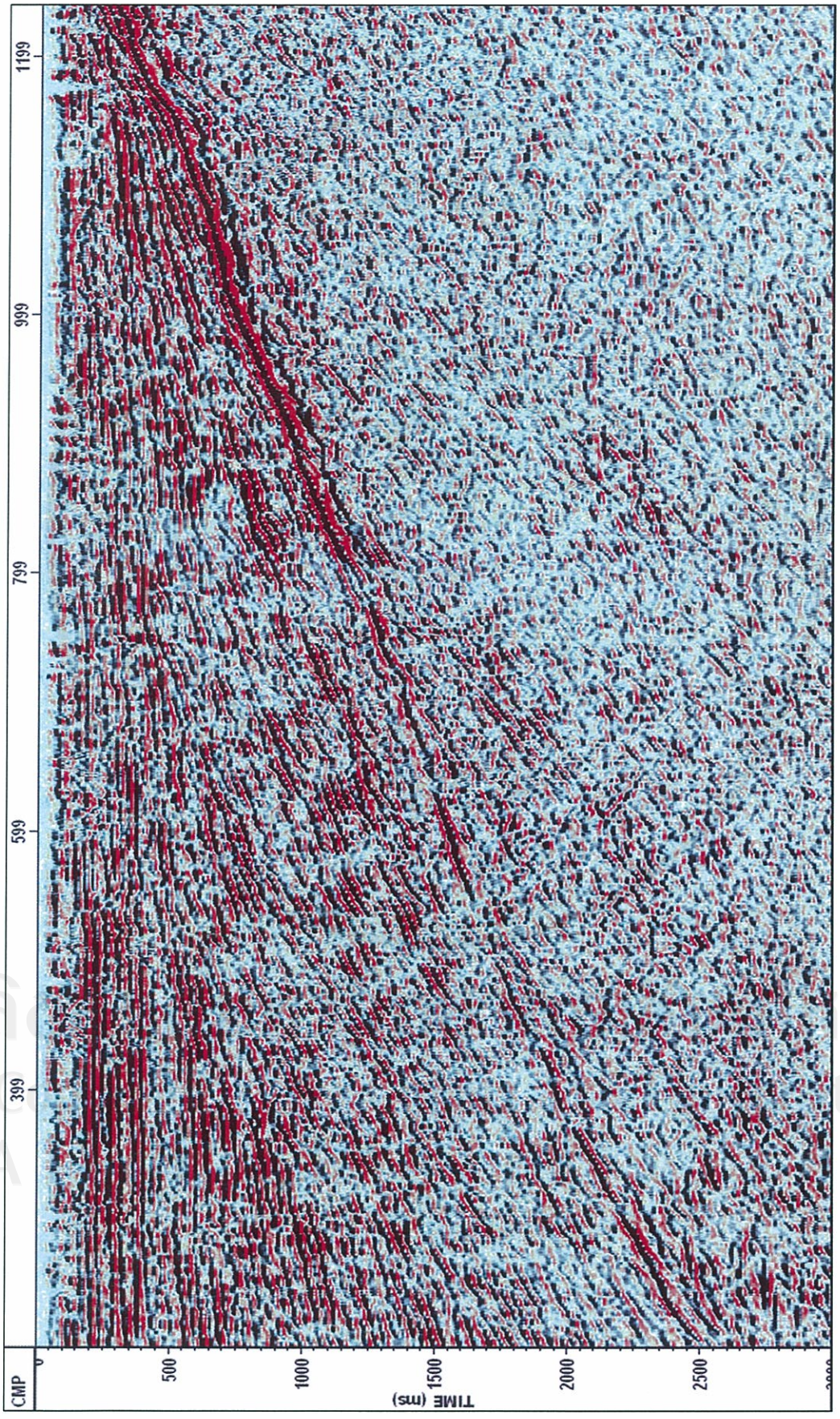

Figure 4.13 Residual static applied final stack section of real data after parabolic *tau-p* processing.

4.3 Result comparison

The result of the conventional processing, the linear *tau-p* processing and the parabolic *tau-p* processing are compared with data after *f-k* filter by presentation in the same parameters display in common shot record (Figure 4.14), velocity energy spectrum (Figure 4.15) and brute stack section (Figure 4.16).

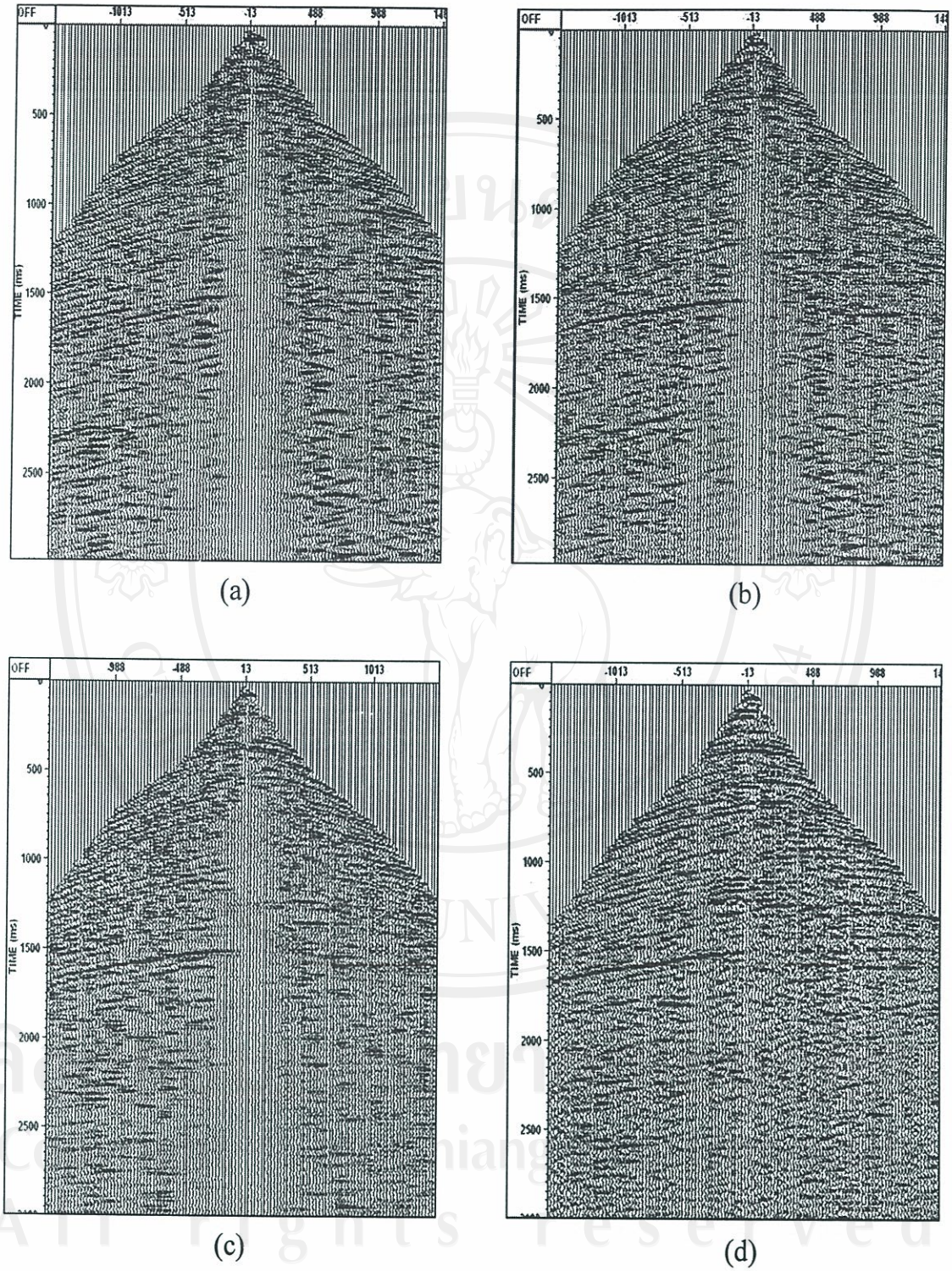

Figure 4.14 Comparing common shot record where (a) after *f-k* filter, (b) conventional processing, (c) linear *tau-p* processing and (d) parabolic *tau-p* processing.

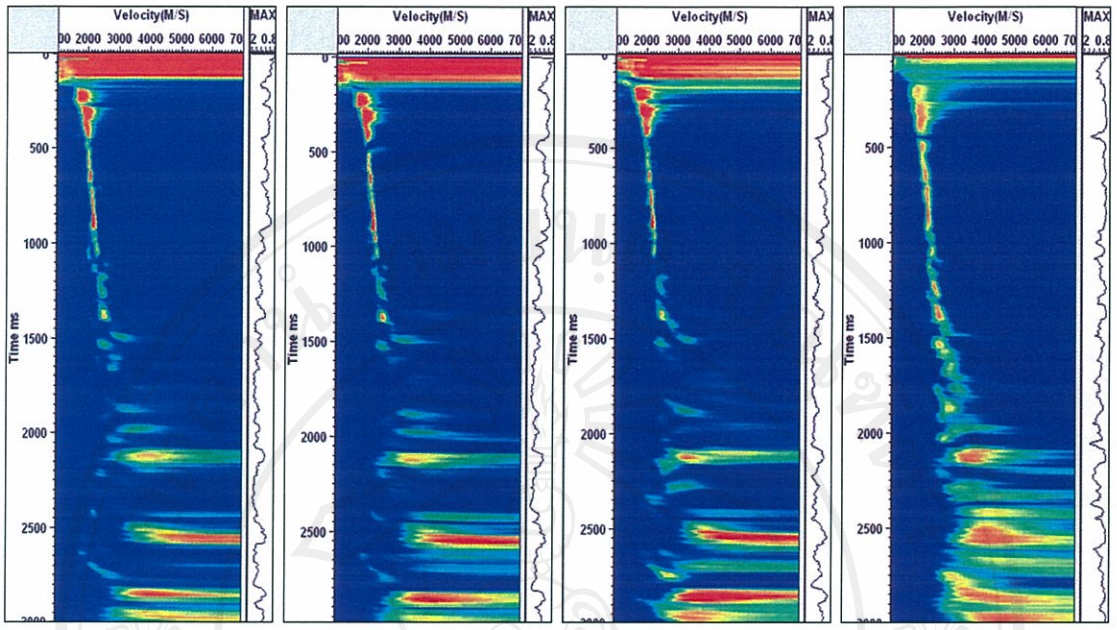

Figure 4.15 Comparing velocity energy spectrum where (a) after *f-k* filter, (b) conventional processing, (c) linear *tau-p* processing and (d) parabolic *tau-p* processing.

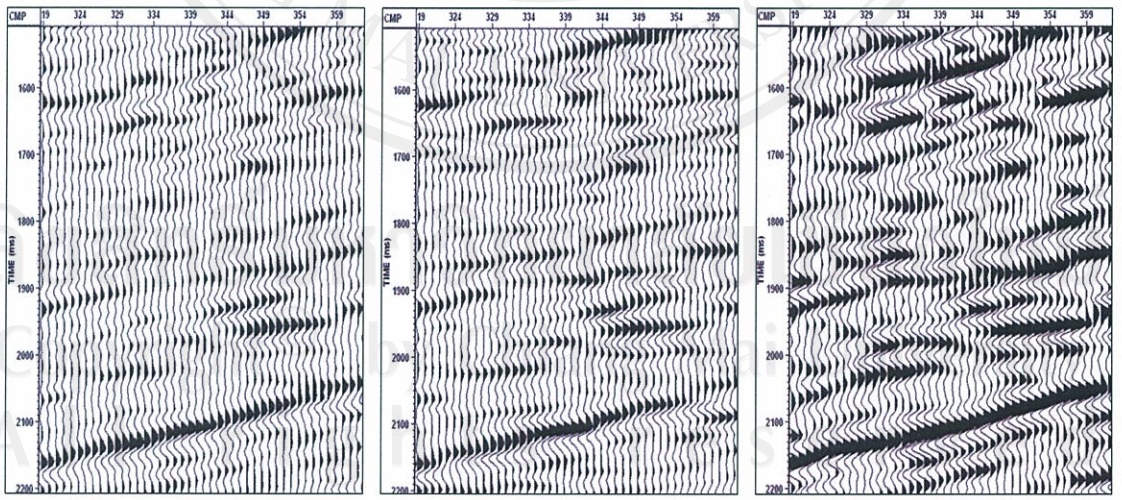

Figure 4.16 Compare brute stack section where (a) conventional processing, (b) linear *tau-p* processing and (c) parabolic *tau-p* processing.